

Power law decay of entanglement quantifiers in a single agent to a many body system coupling.

Ohad Shpielberg^{1,*}

¹*Haifa Research Center for Theoretical Physics and Astrophysics,
University of Haifa, Mt. Carmel, Haifa 31905, Israel*

(Dated: September 21, 2021)

Control over a many body quantum system can be achieved by entangling the system to a single agent. Here, we study the ground state entanglement properties of two site lattice models, between a highly occupied subsystem (site A) to a few particles (site B). Both the Von Neumann entanglement entropy and the Logarithmic negativity show a power law decay in R – the occupancy ratio between the systems. This implies that it is feasible to entangle large many body systems to a single atom, as recently reported experimentally.

I. INTRODUCTION

Entanglement is a key resource in quantum information [1–3], quantum computing [4, 5] and quantum metrology [6]. Recently, there has been significant advancement in generating, manipulating and measuring entangled many body states; both experimentally and theoretically [7–10]. Both preparation of the entangled state and its validation using, e.g. entanglement witnesses [11], are challenging aspects in many body systems and are the focus of ongoing research [12–15].

Preparation of a desired entangled state can be realized as the ground state of a carefully designed Hamiltonian. Therefore, understanding the entanglement properties of ground states is of practical importance. Significant effort has been directed for extended systems, especially in $1D$. The ground state of a Hamiltonian with local interactions typically exhibits an area law in the bipartite Von Neumann entanglement entropy [16], contrary to the generic volume law of typical quantum states. However, the area law does not characterise a system composed of a few sites, where each site can occupy a large number of particles (see Fig. 1). For two sites, the average Von Neumann entanglement entropy is known [17, 18], but the ground state entanglement properties are not.

A particularly appealing case is for a single agent in system B to be entangled to a large number of particles in system A . Such entanglement allows to manipulate the many body system via the single agent. This setup was experimentally demonstrated in [19], where a single photon was entangled with roughly 3,000 atoms. At this point, it is unknown whether there is a limit to the number of particles that could realistically be entangled with a single agent. It is further unknown whether our setup leads to typical ground state entanglement properties.

To answer the above questions, the entanglement needs to be quantified [20, 21]. Choosing an appropriate entanglement quantifier depends on the intended application, e.g. entanglement distillation to produce Bell states.

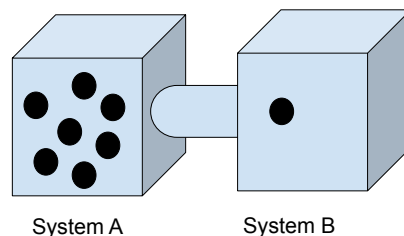


FIG. 1. The systems A and B are made to interact such that we find a large occupancy of particles at system A and a low occupancy at system B .

However, the entanglement quantifier can alternatively be chosen to accommodate fast calculations of known density matrices, e.g. the Logarithmic negativity E_{ln} . For pure states, the Von Neumann entanglement entropy E_{vn} serves both purposes.

In this work we consider N bosons, occupying a two-site system. We study the ground state entanglement properties when the overwhelming majority of bosons occupy site A (see Fig. 1). To make this statement precise, let $\hat{n}_{A,B}$ be the corresponding number operators. Then, $R = \langle \hat{n}_A \rangle / \langle \hat{n}_B \rangle$ is the ratio of the particle occupancies. We study the large R behaviour of both the ground state Von Neumann entanglement entropy and Logarithmic negativity of the Bose-Hubbard Hamiltonian. Then, we study the steady state Logarithmic negativity of a Lindblad super-operator model – the quantum asymmetric inclusion process at large R values [22, 23].

Both models are studied at different scaling regimes. Nevertheless, they all consistently lead to a power law decay in the entanglement quantifiers. Quantitatively, the Von Neumann entanglement entropy $E_{vn} \sim \frac{\log R}{R^\alpha}$ and the Logarithmic negativity $E_{ln} \sim \frac{1}{R^\alpha}$ for $R \gg 1$. See Tables I and II for a summary of the results.

The power law decay seem to be typical as we have considered two disparate models and different scaling

* ohads@sci.haifa.ac.il

regimes for each model. The slow power law decay, contrasting with an exponential decay, suggests it is realistic to entangle a single atom to a highly occupied many body state. The exponent α is non-universal. Therefore, interacting systems that result in small α values are favorable to facilitate entanglement between the single atom to the large occupancy system.

The structure of this paper is as follows. In Sec. II we present the Hamiltonian and Lindblad models and summarise the main results. Sec. III presents in full the analytical and numerical treatment of the systems under study. Finally, Sec. IV recaps the main findings and their physical relevance and suggests future directions.

II. MODELS AND RESULTS

The aim of this work is to quantify the bipartite entanglement of a composite AB system at large R values. Therefore, it is natural to study lattice models, where the distinction between the two subsystems is clear cut. In particular, we study lattice models with two sites, A and B .

Two disparate lattice models are considered. First, the ground state entanglement of the Bose-Hubbard model is extensively studied. Second, we consider a generalization of the asymmetric inclusion process [24] to the quantum realm via a Lindblad equation, dubbed here the quantum asymmetric inclusion process (QASIP). We then study the entanglement properties of the steady state.

A. The Bose-Hubbard model

The Bose-Hubbard model is a simple yet rich many body lattice model of spin-less bosons. It allows studying the superfluid-insulator transition [25] and can be experimentally implemented using optical lattices [26, 27]. The two site Bose-Hubbard model is expected to be both analytically tractable and to present typical physical behaviour in terms of the ground state entanglement. Hence, it serves as the starting point of our analysis.

The Bose-Hubbard Hamiltonian is given by

$$H_{BH} = J(\hat{b}_A^\dagger \hat{b}_B + \hat{b}_B^\dagger \hat{b}_A) - \mu \hat{n}_A + \frac{U}{2} \sum_{i=A,B} \hat{n}_i - \hat{n}_i^2, \quad (1)$$

where J is the hopping matrix element between neighboring sites and U determines the strength of the on-site interaction. The operators $\hat{b}_i, \hat{b}_i^\dagger$ are the site-dependent bosonic creation and annihilation operators and $\hat{n}_i = \hat{b}_i^\dagger \hat{b}_i$ is the number operator for $i = A, B$. In the optical lattice, the potential wells are represented by the two sites [26]. The potential offset between the two potential wells is given by μ . It furthermore allows to imbalance the system towards large R values.

It is useful to note that the total particle number, $\hat{N} = \hat{n}_A + \hat{n}_B$ is conserved. Therefore, we analyze the ground

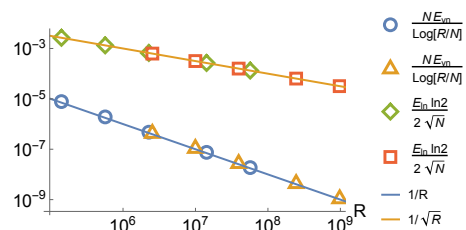


FIG. 2. The scaling of the entanglement at large R for $N = 7$ and $\mu \in [5 \times 10^2, 10^4]$ in the Bose-Hubbard model. The Von Neumann entanglement entropy and the Logarithmic negativity are shown to collapse to $\frac{NE_{ln}}{\ln(R/N)} = 1/R$ and $\frac{E_{ln} \ln 2}{2\sqrt{N}} = 1/\sqrt{R}$ for the values $(J, U) = (1.325, -0.3245)$ (blue circles and green diamonds) and $(J, U) = (0.32, 1.65)$ (orange triangles and red squares). Other U, J values as well as different N were considered, further validating the results.

state with N bosons. In what follows, we consider two scaling schemes leading to large R values.

First, taking large μ values and keeping N, J and U fixed, we find that $R = \mu^2/J^2 + O(\mu)$. In this limit, and as long as $\frac{J\sqrt{N}}{\mu}, \frac{UN^2}{\mu} \ll 1$, we find analytically the power law behaviour described in Table I. These results are also numerically corroborated in Fig. 2. Note that the logarithmic correction in the Von Neumann entanglement hardly changes the behaviour from a clean power law.

Second, we consider the large N limit, with fixed μ, J and U . A perturbative approach is harder in this case. Therefore, we studied the scaling limit numerically, leading to different scaling exponents of the power law behaviour. See Fig. 3. The results for the large N limit are also summarised in Table I. Contrary to the large μ case, the prefactor Γ of the power law (see Table I) was not pursued in the large N limit. Moreover, the value of the exponent changes appreciably when different values of μ, J, U are tested. Further analytical and numerical work is required to find the exponents and prefactors of the large N limit. However, the power law behaviour is unequivocal.

	R	$E_{vn} = \Gamma \frac{\ln R}{R^\alpha}$	$E_{ln} = \frac{\Gamma}{R^\alpha}$
$\mu \gg 1$	μ^2/J^2	$\Gamma = N, \alpha = 1$	$\Gamma = \frac{2\sqrt{N}}{\ln 2}, \alpha = \frac{1}{2}$
$N \gg 1$	$\propto N^\beta, \beta \approx 2.03$	$\alpha \approx 0.548$	$\alpha \approx 0.247$

TABLE I. The power law behaviour of the ground state entanglement of the Bose-Hubbard model at large R values. For the large N limit, the (parameter dependent) exponents are given for $(U, J, \mu) = (0.354, 1.321, 0.875)$.

In conclusion, the ground state of the two site Bose-Hubbard model leads to a power law behaviour of both the Von Neumann entanglement entropy and the Logarithmic negativity at large R values in two different scal-

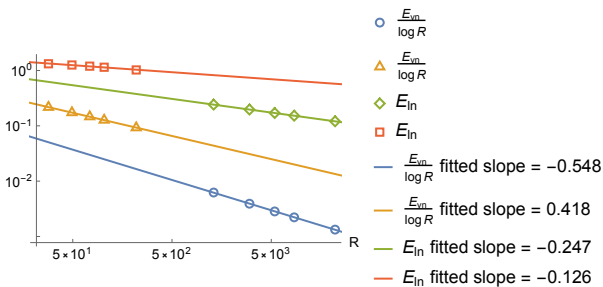


FIG. 3. The scaling of the entanglement at large R for $N \in [10, 40]$ for $(J, U, \mu) = (0.354, 1.321, 0.875)$ (blue circles and green diamonds) and $(J, U, \mu) = (0.763, 0.222, 1.12)$ (orange triangles and red squares). It is evident that the two different sets of values give the expected power law behaviour. The exponent for both the Von Neumann entropy and for the Logarithmic negativity depends on the values of J, U, μ .

ing schemes.

Next, we explore the large R entanglement in an open quantum system setup: the quantum asymmetric inclusion process.

B. Open quantum system

Realistically, physical systems are never truly isolated. Interestingly, the coupling of a quantum system to an environment does not always lead to complete loss of entanglement in the system. Indeed, there are examples where the environment can be engineered to produce a desirable entangled state [15, 28].

Here, we aim to study whether the large R power law behaviour persists for open quantum systems as well. To that end, we focus on a quantum analog of the asymmetric inclusion process given in terms of the Lindblad equation.

In this setup, one usually assumes that a quantum system is coupled to an environment with fast relaxation times. This in turn, allows to discard non-Markovian contributions to the evolution of the density matrix and results in the Lindblad equation [29–31]

$$\begin{aligned} \partial_t \rho &= \mathcal{H}(\rho) + \sum_k \mathcal{D}_{\hat{L}_k}(\rho) \\ \mathcal{H}(\rho) &= -i[H, \rho] \\ \mathcal{D}_{\hat{L}}(\rho) &= \hat{L}\rho\hat{L}^\dagger - \frac{1}{2}\{\hat{L}^\dagger\hat{L}, \rho\}. \end{aligned} \quad (2)$$

In (2), H is a Hermitian operator and $[\bullet, \bullet], \{\bullet, \bullet\}$ are the commutation and anti-commutation relations correspondingly. Despite the restriction to Markovian dynamics, enough quantumness remains in the Lindblad equation [32–34].

The QASIP describes the dynamics of bosons on a two site lattice, where the boson interactions are environment

assisted. The evolution of the density matrix is given by

$$\begin{aligned} \partial_t \hat{\rho} &= \mathcal{L}_{QASIP}(\hat{\rho}) \\ \mathcal{L}_{QASIP}(\hat{\rho}) &= \mathcal{H}_{\text{tb}}(\hat{\rho}) + \mathcal{L}_{\text{D}}(\hat{\rho}) + \mathcal{L}_{\text{E}}(\hat{\rho}) \\ \mathcal{H}_{\text{tb}}(\hat{\rho}) &= \varepsilon \left(\hat{b}_A^\dagger \hat{b}_B + \hat{b}_B^\dagger \hat{b}_A \right) \\ \mathcal{L}_{\text{D}}(\hat{\rho}) &= \eta \sum_{k=A,B} \mathcal{D}_{\hat{n}_k}(\hat{\rho}) \\ \mathcal{L}_{\text{E}}(\hat{\rho}) &= \gamma \mathcal{D}_{\hat{b}_A^\dagger \hat{b}_B}(\hat{\rho}). \end{aligned} \quad (3)$$

Here, the Hermitian H_{tb} is a tight-binding Hamiltonian, \mathcal{L}_{D} is responsible for dephasing at each site and \mathcal{L}_{E} explicitly breaks the symmetry between the two sites and induces the occupation imbalance. Later on, it will be shown that controlling γ allows to induce large R values.

The relation of eq.(3) to the classical ASIP is as follows. The dephasing and bias terms alone acting on the diagonal terms of the density matrix in the number basis lead to the ASIP master equation. Namly, the quantum master equation is split to the diagonal terms and the coherent terms, each having a closed set of equations (in the number operator basis). The tight-binding Hamiltonian mixes between the coherent terms and the diagonal terms, hence a quantum ASIP.

Three comments are in order before we present the results. First, note that here one cannot assume a priori that the quantum system is coupled to a series of thermalized baths as we have not performed a microscopic derivation of the Lindblad equation. Since we are not interested in studying thermalization, the lack of a microscopic derivation is of no importance. Second, the steady state density matrix is not pure. Hence, we will only use the Logarithmic negativity as an entanglement quantifier. Third, in (3) we have set \hbar to unity. Furthermore, we will assume $\varepsilon, \eta, \gamma$ and the time t to be dimensionless for convenience. When presenting the different scaling schemes, the inverse time dimensions of $\varepsilon, \eta, \gamma$ could be restored.

The QASIP, like the Bose-Hubbard model can be shown to conserve the particle number $\hat{N} = \hat{n}_A + \hat{n}_B$ (see the appendix B). However, a related but more general property exists for the QASIP. In the number operator basis, we can write the density matrix as

$$\begin{aligned} \hat{\rho} &= \sum_S a_S \hat{\rho}_S, \quad \text{where} \\ \hat{\rho}_S &= \sum_{x,y=0}^S \varrho_S(x,y) |x, S-x\rangle \langle y, y-S|. \end{aligned} \quad (4)$$

Here, S takes non-negative integer values and a_S are non-negative prefactors that sum to 1. Note that the hermiticity of the density matrix $\hat{\rho}_S$ implies $\varrho_S^*(x,y) = \varrho_S(y,x)$ and unity trace implies $\sum_{x=0}^S \varrho_S(x,x) = 1$.

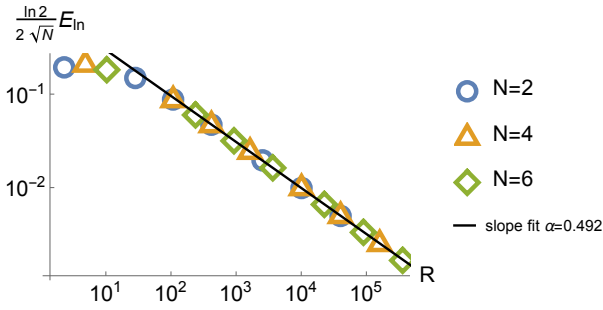


FIG. 4. The scaled Logarithmic Negativity for the QASIP with $\varepsilon = \eta = 1, \gamma \in [1, 200]$ and different N values. The points collapse in the large R limit onto a power law plot. The exponent is in accord with the analytical value of $\alpha = 1/2$.

The dynamics (3) conserves the subspace S

$$\begin{aligned} \partial_t \varrho_S(x, y) = & -\eta(x-y)^2 \varrho_S(x, y) \\ & + \gamma x_- y_- \varrho_S(x-1, y-1) \\ & - \frac{1}{2} \gamma (x_+^2 + y_+^2) \varrho_S(x, y) \\ & - i\varepsilon \sum_{z=\pm 1} x_z \varrho_S(x+z, y) - y_z \varrho_S(x, y+z) \\ X_+ = & \sqrt{(X+1)(S-X)} \\ X_- = & \sqrt{X(S-X+1)}, \quad \text{where } X = x, y. \end{aligned} \quad (5)$$

Namely, we have replaced the treatment of the infinite dimensional density matrix $\hat{\rho}$, with a treatment of finite dimensional $(S+1)^2$ density matrices $\hat{\rho}_S$ at fixed S .

The conserved number S of $\hat{\rho}_S$ equals the number of particles in the system as

$$\text{Tr } \hat{\rho}_S \hat{N} = \sqrt{\text{Tr } \hat{\rho}_S \hat{N}^2} = S. \quad (6)$$

The eq.(5) implies therefore that the process conserves the particle number. From hereon out, we replace S by N .

In (3), there are different scaling schemes leading to the large R limit. The Table II summarises the power law behaviour of the Logarithmic negativity in three different scaling regimes. The results in Table II were verified both analytically and numerically. See Fig.4, 8 and 9 for the large γ limit, and Fig. 5, 10 and 11 for the large η limit. For the large N only numerical evidence is currently present, see Fig. 6 and 12.

In conclusion, the steady state QASIP in eq.(3) exhibits a power law decay in the Logarithmic negativity, similarly to the Bose-Hubbard dynamics.

In the next section, we provide a detailed derivation of the results for the Bose-Hubbard model and for the QASIP.

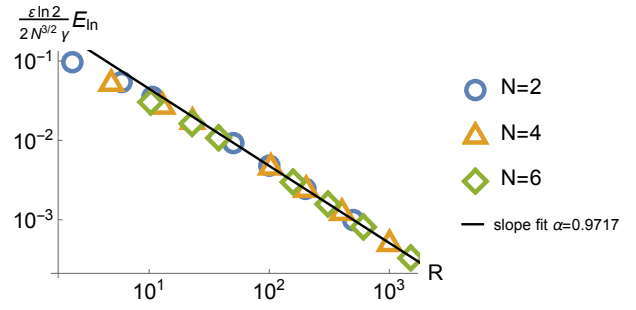


FIG. 5. The scaled Logarithmic Negativity for the QASIP with $\varepsilon = \gamma = 1, \eta \in [1, 500]$ and different N values. The points collapse in the large R limit onto a power law plot. The exponent is in accord with the analytical value of $\alpha = 1$.

	R	$E_{\ln}(R) = \Gamma R^{-\alpha}$
$\gamma \gg 1$	$\frac{\gamma^2 N^2}{4\varepsilon^2}$	$\Gamma = \frac{2\sqrt{N}}{\ln 2}, \quad \alpha = 1/2$
$\eta \gg 1$	$\eta \frac{N\gamma}{2\varepsilon^2}$	$\Gamma = \frac{2N^{3/2}\gamma}{\varepsilon \ln 2}, \quad \alpha = 1$
$N \gg 1$	$\propto N^\beta, \beta \approx 1.941$	$\alpha \approx 0.154$

TABLE II. The power law behaviour of the Logarithmic negativity in the steady state QASIP. For the large N limit, the (parameter dependent) exponents are given for $(\varepsilon, \eta, \gamma) = (1, 1, 1)$.

III. ANALYTICAL AND NUMERICAL ANALYSIS

In Sec. II, we have introduced two lattice models: the Bose-Hubbard model and the quantum asymmetric inclusion process. The power law behaviour of the Von Neumann entanglement and the Logarithmic negativity was summarized in Tables I and II. In this section, we describe the analysis of these results in detail.

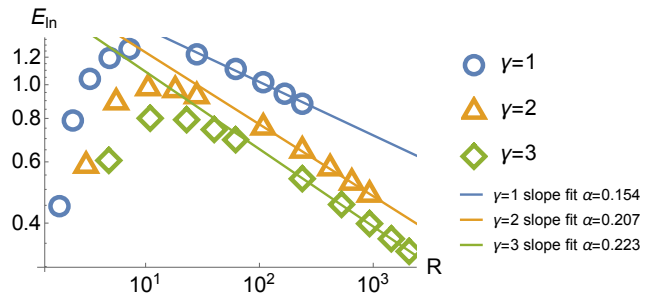


FIG. 6. The Logarithmic Negativity for the QASIP with $\varepsilon = \eta = 1, \gamma = \{1, 2, 3\}$ and $N \in [1, 30]$. The power law form at large R values is unequivocal, however the exponent α is imprecise as the N values are not large enough. Nevertheless, it is clear that the exponent depends on γ .

A. Bose-Hubbard model

To analyze the entanglement properties of the two site Bose-Hubbard model of eq.(1), we need to find the N -particle ground state of the Hamiltonian. Given a description of the ground state, finding the ratio R and the entanglement quantifiers E_{vn}, E_{ln} becomes straightforward, but sometimes technically cumbersome. See the appendix A.

The Hilbert space of N particles for the Bose-Hubbard Hamiltonian eq.(1) is spanned by the $N + 1$ Fock states $|n_A, n_B\rangle = \frac{1}{n_A!n_B!}(\hat{b}_A)^{n_A}(\hat{b}_B)^{n_B}|0, 0\rangle$. Namely,

$$|\psi_N\rangle = \sum_{k=0}^N a_k |k, N-k\rangle, \quad \text{where} \quad \sum_{k=0}^N |a_k|^2 = 1. \quad (7)$$

Then, the N particle Bose-Hubbard Hamiltonian can be written as a $N + 1 \times N + 1$ matrix. Finding the ground state can be done analytically and for all μ, U, J values when we set $N = 1$. This simple case will reveal the intuitive scaling limits leading to the large R behaviour, both for the Bose-Hubbard model as well as for the quantum asymmetric inclusion process in the next subsection.

Indeed, for $N = 1$, the Bose-Hubbard Hamiltonian can be represented by the 2×2 matrix

$$H_{BH}^{(N=1)} = \begin{pmatrix} -\mu & -J \\ -J & 0 \end{pmatrix} \quad (8)$$

where the wavefunction is in its most general form

$$|\psi_{N=1}\rangle = \cos \zeta |10\rangle + e^{i\phi_1} \sin \zeta |01\rangle = \begin{pmatrix} \cos \zeta \\ e^{i\phi_1} \sin \zeta \end{pmatrix} \quad (9)$$

for real ζ, ϕ_1 values and the right hand side of (9) is in a vector notation corresponding to the matrix (8). Clearly, the ratio is $R = \cot^2 \zeta$. The lowest eigenvalue of (8) is $\epsilon = -\frac{1}{2}(\mu + \sqrt{\mu^2 + 4J^2})$ with the ground state $|\psi_{N=1}\rangle = \frac{1}{\mathcal{N}}(-\epsilon|10\rangle + J|01\rangle)$ and \mathcal{N} is a normalization constant. This implies that $R = \epsilon^2/J^2$. Therefore, in this particular case, $R \gg 1$ only if $\mu/J \gg 1$ and leads to $R = (\mu/J)^2 + O(\mu)$ asymptotically.

The Von Neumann entanglement for the ket state (9) is

$$E_{vn} = -2 \cos^2 \zeta \ln(\cos \zeta) - 2 \sin^2 \zeta \ln(\sin \zeta). \quad (10)$$

Using trigonometric identities, we recover $\cos^2 \zeta = \frac{1}{1+R}$ and $\sin^2 \zeta = \frac{R}{1+R}$. Asymptotically for large R , $E_{ln} = \frac{\ln R}{R} + O(R^{-2})$ as reported in I.

To find the Logarithmic negativity, we need to write the partially transposed density matrix

$$\rho^{PT} = \cos^2 \zeta |10\rangle \langle 10| + \sin^2 \zeta |01\rangle \langle 01| + \cos \zeta \sin \zeta (e^{i\phi_1} |01\rangle \langle 01| + e^{-i\phi_1} |10\rangle \langle 10|). \quad (11)$$

The eigenvalues of the partially transposed density matrix are $\cos^2 \zeta, \sin^2 \zeta$ and $\pm i \frac{\sqrt{\cos 4\zeta - 1}}{2\sqrt{2}}$. Therefore, the

Logarithmic negativity is $E_{ln} = \log_2(1 + \frac{\sqrt{\cos 4\zeta - 1}}{\sqrt{2}})$. For large R and to leading order, we find $E_{ln} = \frac{2}{\ln 2} R^{-1/2} + O(R^{-1})$ as reported in Table I.

For $N > 1$, the ground state solution becomes cumbersome, but still requires dealing with a $N + 1 \times N + 1$ Bose-Hubbard matrix. The numerical code that produced Fig. 2,3 and 7 finds the ground state of the Bose-Hubbard matrix at some finite N . Then, it calculates the Von Neumann entanglement and the Logarithmic negativity.

From the $N = 1$ example, we have seen that the large μ limit leads to a large bias $R \gg 1$. For large μ values the particles are similarly biased to occupy site A . This happens when the μ term dominates the energy of the ground state, i.e. for $\mu \gg \sqrt{N}J, UN^2$. Another large R limit is recovered for finite $\mu, U, J > 0$ and large N . In this limit, the particles condense due to the strong attractive energy $\sim UN^2$. The symmetry is broken by the potential offset μ , leading to condensation of the particles in site A and to large R values.

A perturbative approach for the large N limit is non-trivial due to closing of the gapped Hamiltonian. However, a direct numerical analysis clearly reveals the power law behaviour in this limit. See Table I, Sec.II and the appendix C for more details. In what follows, we consider the large μ limit and evaluate the ground state and the entanglement quantifiers using a perturbative approach.

Let us develop a standard perturbation theory for the Hamiltonian $H = H_0 + \frac{1}{\mu}H_1$

$$H_0 = -\hat{n}_A \quad H_1 = H_{BH} - \mu H_0, \quad (12)$$

at large μ .

The eigenstates of H_0 are $|\phi_n^{(0)}\rangle = |n, N-n\rangle$ with energies $\epsilon_n^{(0)} = -n$. The first order correction to the ground state is

$$|\phi_N\rangle = |N, 0\rangle + \lambda |N-1, 1\rangle + O(\lambda^2) \quad (13)$$

where $\lambda = \frac{J\sqrt{N}}{\mu}$ assumed to be small as well as $UN^2/\mu \ll 1$. At this limit we find $R = \langle \hat{n}_A \rangle / \langle \hat{n}_B \rangle = N/\lambda^2$. So, we can approximate at small λ , $R = \mu^2/J^2 + O(\mu)$. The Von Neumann entanglement can be calculated for the ground state $|\phi_N\rangle$

$$E_{vn} = -\frac{1}{1+\lambda^2} \log \frac{1}{1+\lambda^2} - \frac{\lambda^2}{1+\lambda^2} \log \frac{\lambda^2}{1+\lambda^2} \quad (14)$$

$$= -\lambda^2 \log \lambda^2 + O(\lambda^3).$$

At this limit, we find the reported scaling

$$E_{vn} = \frac{N \log R/N}{R}. \quad (15)$$

This is corroborated numerically in Fig. 2 and summarised in Table I. Recall that in this scaling, N may be large, but $R \gg N$.

To find the Logarithmic negativity, we need to calculate the eigenvalues of the partially transposed density

matrix of $|\phi_N\rangle$. For $N > 1$, the only non-zero eigenvalues are $\frac{1}{1+\lambda^2}$, $\frac{\lambda^2}{1+\lambda^2}$, $\frac{\pm\lambda}{1+\lambda^2}$. This leads to

$$E_{ln} = \log_2 \left(1 + \frac{2\lambda}{1+\lambda^2} \right) \approx \frac{2}{\ln 2} \sqrt{\frac{N}{R}}. \quad (16)$$

For large R values, where the perturbation theory applies, the Logarithmic negativity dominates the Von Neumann entanglement as it should [21, 35]. Again, we refer to Fig. 2 to see the excellent agreement with the numerical evaluation.

Other scaling schemes, leading to large R values can exist. Nevertheless, the power law behaviour of the entanglement quantifiers is believed to persist, based on the $N = 1$ exactly solvable cases.

We turn to study the large R entanglement properties of a completely different setup – the quantum asymmetric inclusion process.

B. The QASIP

To analyze the entanglement properties of the QASIP at large R , we need to find the steady state density matrix with a fixed S , i.e. $\mathcal{L}_{QASIP}(\hat{\rho}_S) = 0$. Namely, we wish to find $\varrho_S(x, y)$ such that the right hand side of (5) vanishes.

As in the Bose-Hubbard model, it is useful to study first the simple case of $S = 1$. Here, $x, y = \{0, 1\}$ and demanding a steady state in (5) leads to

$$\begin{pmatrix} -\gamma & i\varepsilon & -i\varepsilon & 0 \\ i\varepsilon & -\frac{1}{2}\gamma - \eta & 0 & -i\varepsilon \\ -i\varepsilon & 0 & -\frac{1}{2}\gamma - \eta & i\varepsilon \\ \gamma & -i\varepsilon & i\varepsilon & 0 \end{pmatrix} \begin{pmatrix} \varrho_1(0, 0) \\ \varrho_1(0, 1) \\ \varrho_1(1, 0) \\ \varrho_1(1, 1) \end{pmatrix} = \begin{pmatrix} 0 \\ 0 \\ 0 \\ 0 \end{pmatrix}. \quad (17)$$

Solving (17), we find the steady state solution for $S = 1$

$$\begin{aligned} \mathcal{N}_1 \hat{\rho}_1 &= 4\varepsilon^2 |0, 1\rangle \langle 0, 1| \\ &+ 2i\gamma\varepsilon (|1, 0\rangle \langle 0, 1| - |0, 1\rangle \langle 1, 0|) \\ &+ (4\varepsilon^2 + \gamma^2 + 2\gamma\eta) |1, 0\rangle \langle 1, 0|. \end{aligned} \quad (18)$$

where $\mathcal{N}_1 = \gamma^2 + 2\gamma\eta + 8\varepsilon^2$ ensures unity trace of $\hat{\rho}_1$. From the steady state solution we recover $R = 1 + \frac{\gamma(\gamma+2\eta)}{4\varepsilon^2}$ and $E_{ln} = \log_2 \left(1 + \frac{4\gamma\varepsilon}{\gamma^2 + 8\varepsilon^2 + 2\gamma\eta} \right)$. A few observations can already be made. At $\eta \rightarrow \infty$ the entanglement vanishes as can be expected in the large dephasing limit [23, 36]. Moreover, the Logarithmic negativity becomes positive due to a combination of biasing and coherent hopping, i.e. $\gamma\varepsilon > 0$. We identify two limits where R becomes large. For $\gamma \rightarrow \infty$ and finite η, ε we recover $R \propto \gamma^2$ and $E_{ln} \propto 1/\sqrt{R}$. Similarly, for finite γ, η and large η we recover $R \propto \eta$ and $E_{ln} \propto 1/R$. Already for the $S = 1$ case we find that the entanglement power law behavior persists for large R values. However, the exponent is non-universal and depends on the scaling scheme.

Exact solution of the steady state for $S > 1$ is at best tedious. Instead, we will find the steady state solution at

two limits noted above, using a perturbative approach; The limits at finite S will be shown to agree with the $S = 1$ exact analysis carried out in the above.

1. Large asymmetry between the sites

For $\gamma \gg 1$, and at finite S, η, ε , we develop the steady state density matrix as a perturbative sum

$$\hat{\rho}_S = \frac{1}{\mathcal{N}_\gamma} (\hat{\rho}_S^{(0)} + \frac{1}{\gamma} \hat{\rho}_S^{(1)} + \frac{1}{\gamma^2} \hat{\rho}_S^{(2)}) + O(1/\gamma^3), \quad (19)$$

where \mathcal{N}_γ is a normalization constant to assure trace one of the truncated density matrix. This perturbative approach implies the order by order steady state solutions

$$0 = \mathcal{L}_E(\hat{\rho}_S^{(0)}) \quad (20)$$

$$0 = \frac{1}{\gamma} \mathcal{L}_E(\hat{\rho}_S^{(1)}) + (\mathcal{L}_D + \mathcal{H}_{tb}) \hat{\rho}_S^{(0)} \quad (21)$$

$$0 = \frac{1}{\gamma} \mathcal{L}_E(\hat{\rho}_S^{(2)}) + (\mathcal{L}_D + \mathcal{H}_{tb}) \hat{\rho}_S^{(1)} \quad (22)$$

Eq.(20) admits a unique solution $\hat{\rho}_S^{(0)} = |S, 0\rangle \langle S, 0|$, namely to leading order site A is maximally occupied and site B is depleted. Using the leading order solution, we find $\hat{\rho}_S^{(1)} = \frac{2i\varepsilon}{\sqrt{S}} (|S, 0\rangle \langle S-1, 1| + |S-1, 1\rangle \langle S, 0|)$. Note that to first order, there are yet no corrections to the occupancies. Hence, we solve to second order in $1/\gamma$ obtaining

$$\begin{aligned} \hat{\rho}_S^{(2)} &= \frac{4\varepsilon^2}{\gamma^2 S} |S-1, 1\rangle \langle S-1, 1| \\ &+ \frac{4i\varepsilon\eta}{S^{3/2}} |S-1, 1\rangle \langle S, 0| \\ &- \frac{2\sqrt{2}\varepsilon^2}{\sqrt{S(S-1)}} |S, 0\rangle \langle S-2, 2| + \text{h.c.} \end{aligned} \quad (23)$$

To second order, we find $\mathcal{N}_\gamma = \frac{4\varepsilon^2}{\gamma^2 S} + 1$. From the perturbative solution (19), we find that

$$R = S - 1 + \frac{S^2 \gamma^2}{4\varepsilon^2} + O(\gamma) \approx \frac{S^2 \gamma^2}{4\varepsilon^2}. \quad (24)$$

This approximation also implies the assumption $\varepsilon^2 \ll S\gamma^2$. Also, the Logarithmic negativity can be calculated as there are at most four non-zero eigenvalue for partially transposed density matrix for any S value. We find to leading order

$$E_{ln} = \frac{4\varepsilon}{\gamma\sqrt{S} \ln 2} + O\left(\frac{1}{\gamma^2}\right) \approx \frac{2\sqrt{S}}{\ln 2} \frac{1}{R} + O\left(\frac{1}{R^2}\right). \quad (25)$$

As noted in Sec. II, the $E_{ln}(R)$ power law behaviour was verified numerically.

2. Large dephasing limit

Here we consider the large η limit with fixed S, γ, ε . As in the large η limit, we write the density matrix as a perturbative series in $1/\eta$

$$\hat{\rho}_S = \frac{1}{\mathcal{N}_\eta} (\hat{\rho}_S^{(0)} + \frac{1}{\eta} \hat{\rho}_S^{(1)} + \frac{1}{\eta^2} \hat{\rho}_S^{(2)}) + O(1/\eta^3), \quad (26)$$

where here \mathcal{N}_η is a normalization constant ensuring the truncated density matrix has trace 1. Again, the perturbative series implies the order by order steady state solutions

$$0 = \mathcal{L}_D(\hat{\rho}_S^{(0)}) \quad (27)$$

$$0 = \frac{1}{\eta} \mathcal{L}_D(\hat{\rho}_S^{(1)}) + (\mathcal{L}_E + \mathcal{H}_{tb}) \hat{\rho}_S^{(0)} \quad (28)$$

$$0 = \frac{1}{\eta} \mathcal{L}_D(\hat{\rho}_S^{(2)}) + (\mathcal{L}_E + \mathcal{H}_{tb}) \hat{\rho}_S^{(1)} \quad (29)$$

Eq.(27) admits a degenerate solution

$$\hat{\rho}_S^{(0)} = \sum_{k=0}^S a_k |k, S-k\rangle \langle k, S-k| \quad (30)$$

with a_k non-negative coefficients. This degeneracy is broken in the next order, i.e. eq.(28). We find $\hat{\rho}_S^{(0)} = |S, 0\rangle \langle S, 0|$, however the degeneracy moves to the next order

$$\begin{aligned} \hat{\rho}_S^{(1)} &= \sum_{k=0}^S b_k |k, S-k\rangle \langle k, S-k| \\ &+ i\varepsilon\sqrt{S} (|S, 0\rangle \langle S-1, 1| - |S-1, 1\rangle \langle S, 0|), \end{aligned} \quad (31)$$

where b_k are again non-negative coefficients. To evaluate to leading order R , we have to break the degeneracy in b_k . This breaking is obtained at the next order, i.e. eq.(29), where we find $b_k = \delta_{k, S-1} \frac{2\varepsilon^2}{\gamma}$ and

$$\begin{aligned} \hat{\rho}_S^{(2)} &= -\frac{\varepsilon^2\sqrt{S-1}\sqrt{S}}{2\sqrt{2}} |S-2, 2\rangle \langle S, 0| \\ &+ i\frac{\gamma^2\varepsilon S^{3/2} + 4\varepsilon^3\sqrt{S}}{2\gamma} |S-1, 1\rangle \langle S, 0| \\ &- i\frac{2\sqrt{2}\varepsilon^3\sqrt{S-1}}{\gamma} |S-2, 2\rangle \langle S-1, 1| \\ &+ \sum_{k=0}^S c_k |k, S-k\rangle \langle k, S-k| \\ &+ \text{h.c.} \end{aligned} \quad (32)$$

The degeneracy in the non-negative terms c_k is broken at the third order of the expansion. To leading order in η , we find $\mathcal{N}_\eta = 1 + \frac{2\varepsilon^2}{\gamma\eta}$. Therefore, to leading order

$$R = \frac{\gamma\eta S}{2\varepsilon^2} + S - 1 \approx \frac{\gamma\eta S}{2\varepsilon^2}. \quad (33)$$

Again, the spectrum of the partially transposed density matrix is composed of only four non-zero eigenvalues for any $S > 1$: $(-\frac{2\gamma\varepsilon\sqrt{S}}{\gamma\eta+2\varepsilon^2}, \frac{2\gamma\varepsilon\sqrt{S}}{\gamma\eta+2\varepsilon^2}, \frac{2\varepsilon^2}{\gamma\eta+2\varepsilon^2}, \frac{\gamma\eta}{\gamma\eta+2\varepsilon^2})$. The Logarithmic negativity is thus given by

$$E_{\text{ln}} = \log_2 \left(1 + \frac{4\gamma\varepsilon\sqrt{S}}{\gamma\eta+2\varepsilon^2} \right) \approx \frac{4\varepsilon\sqrt{S}}{\eta \ln 2} = \frac{2\gamma S^{3/2}}{\varepsilon \ln 2} \frac{1}{R}. \quad (34)$$

C. Large number of particles

We also studied the scaling limit $S \gg 1$ and finite $\eta, \gamma, \varepsilon$. Analytically, a perturbative solution in this case becomes hard due to the closing of the gap. Nevertheless, it is possible to numerically find the steady state and calculate the Logarithmic negativity even for large S values. This was carried out numerically and reported in Sec.II.

IV. DISCUSSION

State of the art experimental techniques allows to entangle a single agent to thousands of atoms [19]. However, it was unclear whether one could push the experimental techniques to significantly increase the number of atoms entangled to the agent.

Here, we have explored the theoretical bounds on entangling one or a few agents to a many body system. The ground state of a two-site Bose-Hubbard model, with an occupancy bias $R \gg 1$ leads to a power law decay in the Logarithmic negativity and the Von Neumann entanglement entropy in different scaling limits. Furthermore, the steady state of the QASIP biased to large R values also exhibits a power law decay in the Logarithmic negativity. We stress that while the power law behaviour is typical, the exponent depends on the scaling limits, see Tables I and II.

From the slow decay of the entanglement, it is now clear why it is possible to entangle thousands of atoms to a single agent. Finding the exact conditions required to attain the observed power law behaviour is an open challenge.

Furthermore, designing systems with slow entanglement decay (small α) allows to entangle more particles in the many body system to the one agent (or a few).

The average Von Neumann entanglement entropy over the random pure state of Hilbert space $N \times N$ is $E_{v_n} \sim \log N$ [17, 18]. Therefore, the Von Neumann entanglement entropy of the ground state is fundamentally different than that of the average. This is not too surprising when one relates to the area law of ground states in extended systems compared to the typical volume law. In turn, the low Von Neumann entanglement entropy of the ground state suggests that ground states in the large R limit could be susceptible to analytical and numerical techniques, even for large many body systems.

From the analysis so far, it may seem that the two-site lattice model is paramount to achieve the power law behaviour. We have carried out preliminary tests in a three site Hubbard model. Taking sites A, B to occupy most of the particles in the system, namely $R = \langle \hat{n}_A + \hat{n}_B \rangle / \langle \hat{n}_C \rangle$. The Von Neumann entanglement entropy between site C and the subsystem AB still exhibits a power law in large R . The analysis is beyond the scope of this work and will be presented elsewhere.

Another question that comes to mind is whether the power law behaviour persists also in continuum models, and not only in lattice models. We believe this is not the case. After coarse graining a lattice model into a continuum model, an increase is expected in the Von Neumann entanglement entropy due to loss of information. This increase does not depend on the occupancies and hence adds a constant to the Von Neumann entanglement entropy. Therefore, in the large R limit we expect to observe a saturation to a constant with a power law correction. Naively, that should be the same power law of the lattice model. It would be interesting to test this conjecture in future works.

Acknowledgments: I would like to thank Guy Cohen, Shahaf Asban and Ofir E. Alon for stimulating talks on the subject.

Appendix A: Entanglement quantifiers

In this section, we provide a short presentation to the entanglement quantifiers used in this text: the Von Neumann entanglement entropy and the Logarithmic negativity. The purpose of quantifiers is to distinguish between entangled states to non-entangled state (separable) and furthermore to suggest a hierarchy of values for entangled states. Here we do not aim to give an exhaustive account of quantum quantifiers, but to motivate the usage of the Von Neumann entanglement entropy and the Logarithmic negativity in the case at hand.

For pure states, all entanglement measures are defined to correspond to the Von Neumann entanglement entropy [21]. In bipartite system AB ,

$$E_{ln}(\rho_{AB}) = -\text{Tr} \rho_A \ln \rho_A = -\text{Tr} \rho_B \ln \rho_B, \quad (\text{A1})$$

where $\rho_A = \text{Tr}_B \rho_{AB}$ is the reduced density matrix. $E_{ln} > 0$ only for non-separable pure states.

In terms of wave functions (which are pure states), the Schmidt decomposition in terms of the orthonormal states implies $|\psi\rangle = \sum_i \alpha_i |u_i\rangle_A \otimes |v_i\rangle_B$. Then, we find $E_{ln}(|\psi\rangle) = -\sum_i |\alpha_i|^2 \log |\alpha_i|^2$.

Entanglement is harder to quantify for mixed states. Many different measures for the entanglement exists. Typically, entanglement measures are given in the form of some minimization problem, making them hard to calculate. Instead, we will use the Logarithmic negativity which is an entanglement monotone and not a measure. Namely, for pure state the Logarithmic negativity does

not correspond to the Von Neumann entanglement entropy (except for specific cases). However, it is straightforward to calculate the Logarithmic negativity, making it a favorable entanglement quantifier.

The Logarithmic Negativity is given by

$$E_{ln}(\rho) = \log_2 \|\rho^{PT}\|_1, \quad (\text{A2})$$

where ρ^{PT} is the partially transposed density matrix, and $\|A\|_1 \equiv \text{Tr} \sqrt{AA^\dagger}$. Intuitively speaking, the Logarithmic negativity counts the amount of negative eigenvalues in the partially transposed density matrix relating it to the Peres–Horodecki criterion [37, 38]. We note that a positive Logarithmic negativity values insures non-separability, but a vanishing value does not guarantees separability.

The Logarithmic Negativity is an entanglement monotone [20, 21, 39], which implies that on average, under locally quantum operations and classical communication (LOCC), the Logarithmic Negativity does not increase. Furthermore, the Logarithmic negativity was shown to be an upper bound for the distillation entanglement, connecting it to useful quantum operations using maximally entangled states [40]. Since the distillation entanglement is an entanglement measure, it is evident that for pure states the the Von Neumann entanglement entropy is bounded by the Logarithmic negativity. This fact provides a consistency check in our numerical assessment.

Appendix B: The Lindblad adjoint dynamics

The purpose of this section is to introduce the Heisenberg operator evolution picture for the Lindblad dynamics.

For an observable \hat{O} (explicitly time-independent), we have the expectation value $\langle \hat{O} \rangle = \text{Tr} \hat{O} \rho$. Therefore,

$$\partial_t \langle \hat{O} \rangle = \text{Tr} \hat{O} \partial_t \rho = \text{Tr} \hat{O} \mathcal{L}(\rho), \quad (\text{B1})$$

where $\mathcal{L}(\rho)$ is a Lindblad super-operator of the form 2. Then, the formal adjoint \mathcal{L}^\dagger is defined such that

$$\partial_t \langle \hat{O} \rangle = \text{Tr} \mathcal{L}^\dagger(\hat{O}) \rho. \quad (\text{B2})$$

For the Lindblad super-operator (2), it implies the Heisenberg picture

$$\partial_t \hat{O} = \mathcal{L}^\dagger(\hat{O}) = -\mathcal{H}(\hat{O}) + \sum_k \hat{L}_k^\dagger \hat{O} \hat{L}_k - \frac{1}{2} \{ \hat{L}_k^\dagger \hat{L}_k, \hat{O} \}. \quad (\text{B3})$$

It is rather straight-forward to see that $\partial_t \hat{N} = 0$ for the QASIP.

Appendix C: Additional numerical data for the Bose-Hubbard model

Here we present further technical details on the numerical analysis of the Bose-Hubbard model.

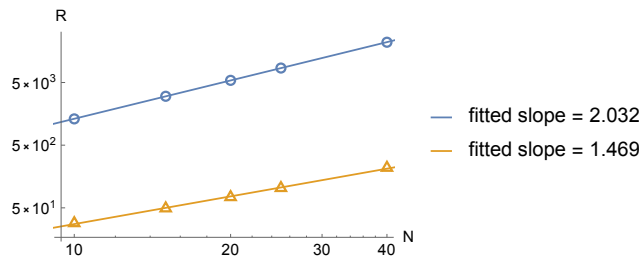


FIG. 7. The scaling of R with N for the Bose-Hubbard model of $N \in [10, 40]$ with the two realizations $(J, U, \mu) = (0.354, 1.321, 0.875)$ and $(J, U, \mu) = (0.763, 0.222, 1.12)$. It is evident that the two different sets of values give different power law behaviour $R \propto N^\beta$ with $\beta \approx 2, 1.47$. Other (J, U, μ) lead to different β exponents.

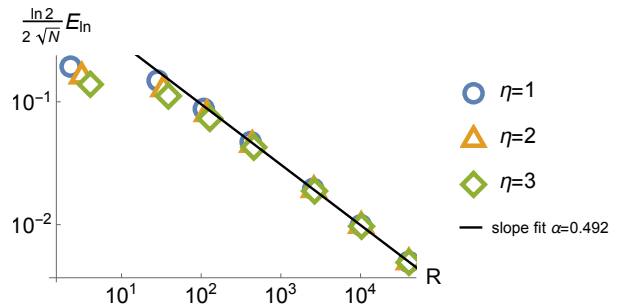


FIG. 8. The scaled Logarithmic Negativity for the QASIP with $\varepsilon = 1, N = 2, \gamma \in [1, 200]$ and different η values. The points collapse in the large R limit onto a power law plot. The exponent is in accord with the analytical value of $\alpha = 1/2$.

In Fig. 7, the scaling $R \sim N^\beta$ for the large N limit is presented for two arbitrary values of (J, U, μ) . It can be seen that β depends on the values (J, U, μ) . Other values were tested, but not shown here, leading to different β values.

Appendix D: Additional numerical data for the QASIP model

Here we present further technical details on the numerical analysis of the QASIP model.

In Fig. 8 and 9 we show the collapse of the scaled Logarithmic negativity at large γ for different η and ε values correspondingly as predicted by the perturbation theory.

In Fig. 10 and 11 we show the collapse of the scaled Logarithmic negativity at large η for different ε and γ values correspondingly as predicted by the perturbation theory.

In Fig. 12 the large N scaling of $R \propto N^\beta$ is plotted for different γ values. It is hard to determine the dependence of the exponent β on the parameters $\gamma, \eta, \varepsilon$, especially since large N values are numerically challenging.

-
- [1] R. Horodecki, P. Horodecki, M. Horodecki, and K. Horodecki, *Rev. Mod. Phys.* **81**, 865 (2009).
 - [2] L. Amico, R. Fazio, A. Osterloh, and V. Vedral, *Reviews of modern physics* **80**, 517 (2008).
 - [3] V. Vedral, *Decoding reality: the universe as quantum information* (Oxford University Press, 2018).
 - [4] M. A. Nielsen and I. Chuang, “Quantum computation and quantum information,” (2002).
 - [5] J. Preskill, *Quantum* **2**, 79 (2018).
 - [6] L. Pezze, A. Smerzi, M. K. Oberthaler, R. Schmied, and P. Treutlein, *Reviews of Modern Physics* **90**, 035005 (2018).
 - [7] A. Omran, H. Levine, A. Keesling, G. Semeghini, T. T. Wang, S. Ebadi, H. Bernien, A. S. Zibrov, H. Pichler, S. Choi, *et al.*, *Science* **365**, 570 (2019).
 - [8] R. Islam, R. Ma, P. M. Preiss, M. E. Tai, A. Lukin, M. Rispoli, and M. Greiner, *Nature* **528**, 77 (2015).
 - [9] A. M. Kaufman, M. E. Tai, A. Lukin, M. Rispoli, R. Schittko, P. M. Preiss, and M. Greiner, *Science* **353**, 794 (2016).
 - [10] S. Kallush, R. Dann, and R. Kosloff, arXiv preprint arXiv:2107.11767 (2021).
 - [11] D. Chruściński and G. Sarbicki, *Journal of Physics A: Mathematical and Theoretical* **47**, 483001 (2014).
 - [12] D. Lacroix, *Physical Review Letters* **125**, 230502 (2020).
 - [13] H. Weimer, M. Müller, I. Lesanovsky, P. Zoller, and H. P. Büchler, *Nature Physics* **6**, 382 (2010).
 - [14] A. Carr and M. Saffman, *Physical Review Letters* **111**, 033607 (2013).
 - [15] F. Verstraete, M. M. Wolf, and J. I. Cirac, *Nature*

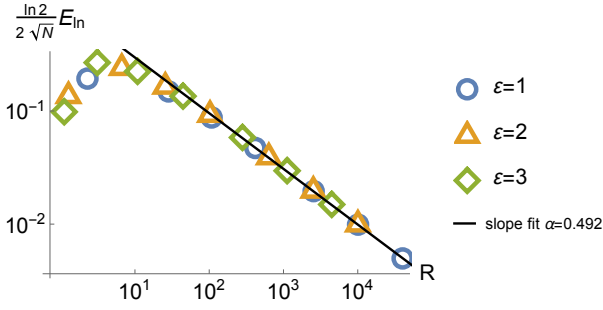


FIG. 9. The scaled Logarithmic Negativity for the QASIP with $\eta = 1, N = 2, \gamma \in [1, 200]$ and different ϵ values. The points collapse in the large R limit onto a power law plot. The exponent is in accord with the analytical value of $\alpha = 1/2$.

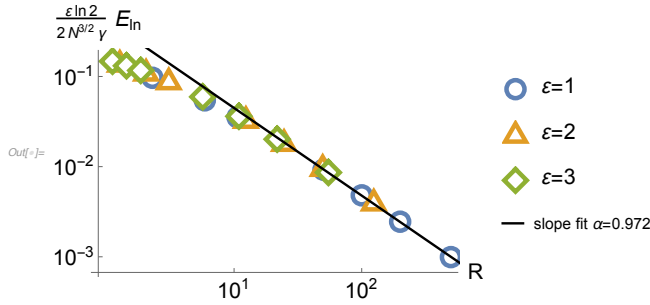


FIG. 10. The scaled Logarithmic Negativity for the QASIP with $N = 2$ and $\gamma = 1, \eta \in [1, 500]$ and different ϵ values. The points collapse in the large R limit onto a power law plot. The exponent is in accord with the analytical value of $\alpha = 1$.

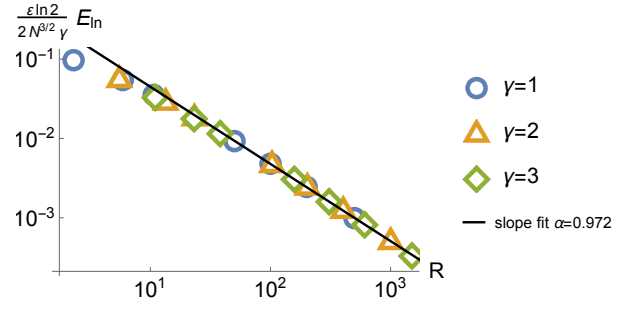


FIG. 11. The scaled Logarithmic Negativity for the QASIP with $N = 2$ and $\epsilon = 1, \eta \in [1, 500]$ and different γ values. The points collapse in the large R limit onto a power law plot. The exponent is in accord with the analytical value of $\alpha = 1$.

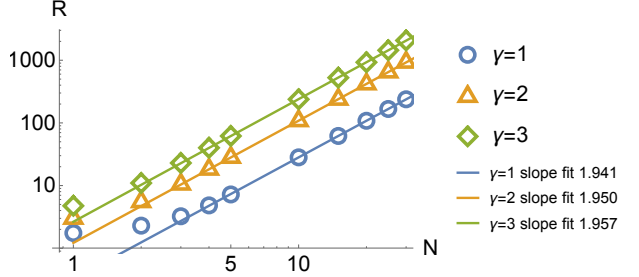


FIG. 12. The scaling of the ratio R with the particle number N for the QASIP, with $\epsilon = \eta = 1$, and different γ values. A close to quadratic scaling is observed.

physics **5**, 633 (2009).

- [16] J. Eisert, M. Cramer, and M. B. Plenio, arXiv preprint arXiv:0808.3773 (2008).
- [17] D. N. Page, Physical Review Letters **71**, 1291 (1993).
- [18] S. Sen, Physical Review Letters **77**, 1 (1996).
- [19] McConnell, R., Zhang, H., Hu, J. et al., Nature **519**, 439–442 (2015).
- [20] N. Friis, G. Vitagliano, M. Malik, and M. Huber, Nat. Rev. Phys. **1**, 72 (2019).
- [21] M. B. Plenio and S. Virmani, Quant.Inf.Comput **7**

- (2007).
- [22] V. Eisler, Journal of Statistical Mechanics: Theory and Experiment **2011**, P06007 (2011).
- [23] D. Bernard, T. Jin, and O. Shpielberg, EPL (Europhysics Letters) **121** (6), 60006 (2018).
- [24] S. Grosskinsky, F. Redig, and K. Vafayi, J. Stat. Phys. **142**, 952 (2011).
- [25] M. P. A. Fisher, P. B. Weichman, G. Grinstein, and D. S. Fisher, Phys. Rev. B **40**, 546 (1989).
- [26] D. Jaksch, C. Bruder, J. I. Cirac, C. W. Gardiner, and P. Zoller, Physical Review Letters **81**, 3108 (1998).
- [27] M. Greiner, O. Mandel, T. Esslinger, T. W. Hänsch, and I. Bloch, nature **415**, 39 (2002).
- [28] O. Shpielberg, EPL (Europhysics Letters) **129**, 60005 (2020).
- [29] Petruccione, F. and Breuer, H.-P., *The Theory of Open Quantum Systems* (Oxford University Press, 2002).
- [30] V. Gorini, A. Kossakowski, and E. C. G. Sudarshan, Journal of Mathematical Physics **17**, 821 (1976).
- [31] G. Lindblad, Communications in Mathematical Physics **48**, 119 (1976).
- [32] Spohn, Herbert and Lebowitz, Joel L., J. Adv. Chem. Phys **38**, 109 (1978).
- [33] Kosloff, Ronnie, Entropy **15** (6), 2100 (2013).
- [34] S. Dutta and N. R. Cooper, Phys. Rev. Lett. **123**, 250401 (2019).
- [35] M. B. Plenio, J. Eisert, J. Dreissig, and M. Cramer, Physical review letters **94**, 060503 (2005).
- [36] M. H. Fischer, M. Maksymenko, and E. Altman, Phys. Rev. Lett. **116**, 160401 (2016).
- [37] A. Peres, Phys.Rev.Lett. **77**, 1413 (1996).
- [38] M. Horodecki, P. Horodecki, and R. Horodecki, Physics Letters A **223**, 1 (1996).
- [39] M. B. Plenio, Phys. Rev. Lett. **95**, 090503 (2005).
- [40] K. Audenaert, M. B. Plenio, and J. Eisert, Phys. Rev. Lett. **90**, 027901 (2003).